

Article

Surface Water Extraction and Dynamic Analysis of Baiyangdian Lake Based on the Google Earth Engine Platform Using Sentinel-1 for Reporting SDG 6.6.1 Indicators

Zijie Jiang ^{1,*}, Weiguo Jiang ^{1,*} , Ziyang Ling ^{2,3}, Xiaoya Wang ¹, Kaifeng Peng ¹ and Chunlin Wang ^{1,3} 

¹ State Key Laboratory of Remote Sensing Science, Faculty of Geographical Science, Beijing Normal University, Beijing 100875, China; jiangzijie@mail.bnu.edu.cn (Z.J.); wangxiaoya@mail.bnu.edu.cn (X.W.); pengkaifeng@mail.bnu.edu.cn (K.P.); wangchunlin@mail.bnu.edu.cn (C.W.)

² School of Geography and Planning, Nanning Normal University, Nanning 530001, China; lingziyan@nnu.edu.cn

³ Beijing Key Laboratory for Remote Sensing of Environment and Digital Cities, Faculty of Geographical Science, Beijing Normal University, Beijing 100875, China

* Correspondence: jiangweiguo@bnu.edu.cn

Abstract: Surface water is an essential element that supports natural ecosystem health and human life, and its losses or gains are closely related to national or local sustainable development. Monitoring the spatial-temporal changes in surface water can directly support the reporting of progress towards the sustainable development goals (SDGs) outlined by the government, especially for measuring SDG 6.6.1 indicators. In our study, we focused on Baiyangdian Lake, an important lake in North China, and explored its spatiotemporal extent changes from 2014 to 2020. Using long-term Sentinel-1 SAR images and the OTSU algorithm, our study developed an automatic water extraction framework to monitor surface water changes in Baiyangdian Lake at a 10 m resolution from 2014 to 2020 on the Google Earth Engine cloud platform. The results showed that (1) the water extraction accuracy in our study was considered good, showing high consistency with the existing dataset. In addition, it was found that the classification accuracy in spring, summer, and fall was better than that in winter. (2) From 2014 to 2020, the surface water area of Baiyangdian Lake exhibited a slowly rising trend, with an average water area of 97.03 km². In terms of seasonal variation, the seasonal water area changed significantly. The water areas in spring and winter were larger than those in summer and fall. (3) Spatially, most of the water was distributed in the eastern part of Baiyangdian Lake, which accounted for roughly 57% of the total water area. The permanent water area, temporary water area, and non-water area covered 49.69 km², 97.77 km², and 171.55 km², respectively. Our study monitored changes in the spatial extent of the surface water of Baiyangdian Lake, provides useful information for the sustainable development of the Xiong'an New Area and directly reports the status of SDG 6.6.1 indicators over time.

Keywords: Baiyangdian Lake; Google Earth Engine; SDG 6.6.1; sentinel-1; OTSU; dynamic changes



Citation: Jiang, Z.; Jiang, W.; Ling, Z.; Wang, X.; Peng, K.; Wang, C. Surface Water Extraction and Dynamic Analysis of Baiyangdian Lake Based on the Google Earth Engine Platform Using Sentinel-1 for Reporting SDG 6.6.1 Indicators. *Water* **2021**, *13*, 138. <https://doi.org/10.3390/w13020138>

Received: 4 December 2020

Accepted: 4 January 2021

Published: 8 January 2021

Publisher's Note: MDPI stays neutral with regard to jurisdictional claims in published maps and institutional affiliations.



Copyright: © 2021 by the authors. Licensee MDPI, Basel, Switzerland. This article is an open access article distributed under the terms and conditions of the Creative Commons Attribution (CC BY) license (<https://creativecommons.org/licenses/by/4.0/>).

1. Introduction

Water resources are one of the basic materials needed for the survival of natural ecosystems and human society. Water supports multiple ecosystem services and provides diverse ecological functions for human activities and biological reproduction and habitat.

Due to climate change and other “global megatrends” such as population increase and urbanization, between 1970 and 2015, inland and marine/coastal wetlands both declined by approximately 35% where data are available, three times the rate of forest loss. [1]. Over the past 30 years, due to the impact of human activities and climate change, the global permanent water area has decreased by 90,000 km², which includes the artificially increased area of reservoirs [2]. The adverse impacts on ecology will significantly deteriorate ecosystem service functions. Thus, monitoring surface water dynamics is necessary

for national or regional sustainable development and is the focus of the United Nations Sustainable Development Goals (SDGs) framework.

To achieve sustainable development that balances natural ecosystem protection and economic growth, the United Nations (UN) drafted the 2030 Agenda for Sustainable Development and proposed 17 Sustainable Development Goals (SDGs), which included 169 targets and 232 indicators. Among them, SDG 6.6.1, which measures the “spatial extent of water-related ecosystems”, is closely related to the surveying of surface water resources. Conventional spatial measurement methods or statistical survey methods, such as field surveying, have the disadvantages of having a high inaccuracy and being largely time-consuming [3]. Remote sensing technology can monitor the spatiotemporal changes in surface water bodies in a scientific, refined, and large-scale manner and can calculate the SDG 6.6.1 indicators more accurately and better serve the goal of achieving SDG 6.6.1. Studies, such as those of Fitoka et al. and Weise et al., based on the SWOS plan, are all aiming to develop spatial mapping methods of the wetland areas and to apply their research results to the calculation and analysis of indicators in SDG 6.6.1 [4,5]. Mulligan et al. used remote sensing and spatial ecosystem service models to determine priority areas for sustainable management at the national and basin scales in the study area and analysed the contribution of nature to SDG 6 [6].

Since the development of remote sensing technology, there have been many freely available public data sources, mainly including optical and radar data, such as Landsat-4/5/7/8, Sentinel-1/2, MODIS, and GF-1/2 [7–10], which have been widely used in water distribution mapping. Optical remote sensing data can realize high-precision water body identification. In recent years, popular water extraction methods include the use of water indexes, such as NDWI, MNDWI, and AWEI, and machine learning algorithms, such as the SVM and random forest (RF) algorithms, which have been widely implemented in optical imaging [11–14]. Hui et al. used MNDWI and multi-time series Landsat images to map the temporal and spatial changes in the Poyang Lake water body and the time course of wetland flooding. Deng et al. used a random forest algorithm to study the dynamic range of lake water in the Wuhan urban agglomeration from 1987 to 2015, and the classification accuracy reached 93.11% [15]. However, many studies have pointed out that for water extraction based on optical images, it is necessary to select images with no or few clouds to avoid the influence of cloud cover as much as possible. Because of this factor, the time resolution of the image is reduced, resulting in no usable images within a month [16–18].

Compared with optical remote sensing data, SAR data can be used in all weather conditions and are sensitive to identified water due to its specular reflection [19,20]. Among them, Sentinel-1 SAR data have become widely used in most studies because of their ease of access and high resolution [21]. Based on SAR images, water extraction methods include experience-based single threshold segmentation, automatic threshold methods, and other classification algorithms [22]. Zeng used the experience-based histogram threshold method to extract the water body of Poyang Lake based on Sentinel-1 data [23]. Markert et al. used the OTSU method to study the effect of Sentinel-1 data processed with and without terrain correction on the results of water body extraction [24]. Zhou et al. used the OTSU method to extract water information using Sentinel-1 data from January 2017 to 2020 and achieved an extraction accuracy of 92% [25]. This study considers the practicability of Sentinel-1 data and aims to extract the Baiyangdian Lake water area using a relatively simple, efficient, and accurate method. Therefore, this research adopts the mature OTSU image segmentation method [26].

In recent years, the Google Earth Engine (GEE) platform has become increasingly widely used. It integrates massive amounts of remote sensing data and has the advantage of rapidly processing and analyzing geospatial data [27]. For example, Pekel et al. used 3 million Landsat remote sensing images to produce a global water distribution map with a 30 m spatial resolution from 1984 to 2015 using the GEE platform [2]. Deng et al. used 75,593 Landsat images to monitor the dynamic changes in open surface open water in the Yangtze River Basin in China from 1984 to 2018 using the GEE platform [28]. Therefore, the

emergence of the GEE cloud platform provides us with new insight into long-term water dynamics in the region.

Baiyangdian Lake, referred to as the pearl of North China, is a largest natural freshwater wetland located in the semiarid plain of North China. Baiyangdian lake is of vital importance to the Xiong'an New Area and even the Beijing–Tianjin–Hebei urban agglomeration. However, due to the influence of climate change and human activities, the surface water of Baiyangdian Lake has undergone significant spatial changes, resulting in significant hydrological, ecological, and economic consequences [29,30]. Therefore, monitoring the dynamic changes in Baiyangdian Lake water distribution is of great significance for improving Beijing's noncapital functions in the future.

The main purpose of our study was to map the surface water of Baiyangdian Lake with high spatial and temporal resolutions and explore its dynamics over a long-term time series. Particularly we aimed to achieve the following goals:

- (1) develop an automatic water extraction framework using long-term Sentinel-1 images and the OTSU algorithm;
- (2) analyse the water extent change of Baiyangdian Lake from October 2014 to May 2020 in support of reporting the SDG 6.6.1 indicators;
- (3) explore the spatiotemporal characteristics of the Baiyangdian Lake extent and discuss the causes of the changes in Baiyangdian Lake.

2. Materials and Methods

2.1. Study Area

The Baiyangdian Wetland (38°43'–39°02' N, 115°38'–116°07' E), the largest lake-type wetland in the Beijing–Tianjin–Hebei urban agglomeration, is located in the central part of the Hebei Province, China, and the administrative region belongs to the Xiong'an New Area in Baoding [30]. Baiyangdian Lake is the most important water function area for maintaining the ecological balance in the Xiong'an New Area [31]. It is a large plain flood depression in the middle reaches of the Daqing River system in the Haihe Basin. It receives nine rivers into its lake from the south, west, and north directions. It belongs to the warm temperate continental monsoon climate, with an average annual rainfall of approximately 550 mm, which is unevenly distributed throughout the year. Rainfall from July to September accounts for 80% of the annual rainfall, and the average annual temperature is 7–12 °C. The annual average evaporation from Baiyangdian Lake is approximately 1369 mm, which is much larger than the precipitation. As shown in Figure 1, Baiyangdian Lake is mainly composed of seven subregions, namely, Zaozhadian (A), Shaochedian (B), Lianhuadian (C), Chiyudian (D), Houtangdian (E), Baiyangzhengdian (F), and Mapengdian (G), comprising over 140 small lakes. It plays a key role in maintaining the regional ecological balance and protecting biodiversity and rare species resources.

2.2. Datasets and Preprocessing

This study collects 251 Sentinel-1 SAR images of Baiyangdian Lake, vector boundary data for the study area, and the Landsat-SMDPSO water dataset based on Landsat data using the SMDPSO algorithm for verification. Among them, the SMDPSO algorithm is an optimization algorithm based on spectral matching and discrete particle swarm optimization using multispectral remote sensing images [32,33]. Using the SMDPSO method, a Landsat-SMDPSO water dataset was produced based on Landsat 7/8. Sentinel-1 is an earth observation satellite in the European Space Agency's Copernicus Project (GMES). It consists of two satellites that were launched in 2014/2016 and carries an imaging system for a C-band synthetic aperture radar [34]. In Baiyangdian Lake, the first Sentinel-1 image was taken on 28 October, 2014. Since only sentinel-1A was in orbit, until June 2015, only one image could be obtained each month. From July 2015 to May 2016, 2–3 available images could be obtained each month. Since the launch of sentinel-1B in June 2016, four to five images could be obtained each month. Therefore, it can ensure the density of image time series in Baiyangdian Lake (Figure 2). On the GEE, free public data is provided. This

study uses dual polarization to provide Level-1 Sentinel-1 GRD products in IW mode as the original data, with a resolution of 10 m*10 m. These data have been preprocessed on the GEE using the Sentinel-1 toolbox using the following steps: (1) orbit file application; (2) GRD border noise removal; (3) thermal noise removal; (4) radiometric calibration; (5) terrain correction using SRTM or ASTER DEM; and (6) terrain corrections conversion to decibels through logarithmic transformation. Finally, a multitemporal Refined Lee speckle filter was used to filter the backscattered time series to minimize the impact of environmental conditions and remove the noise in the Sentinel-1 dataset resulting from speckling [35,36].

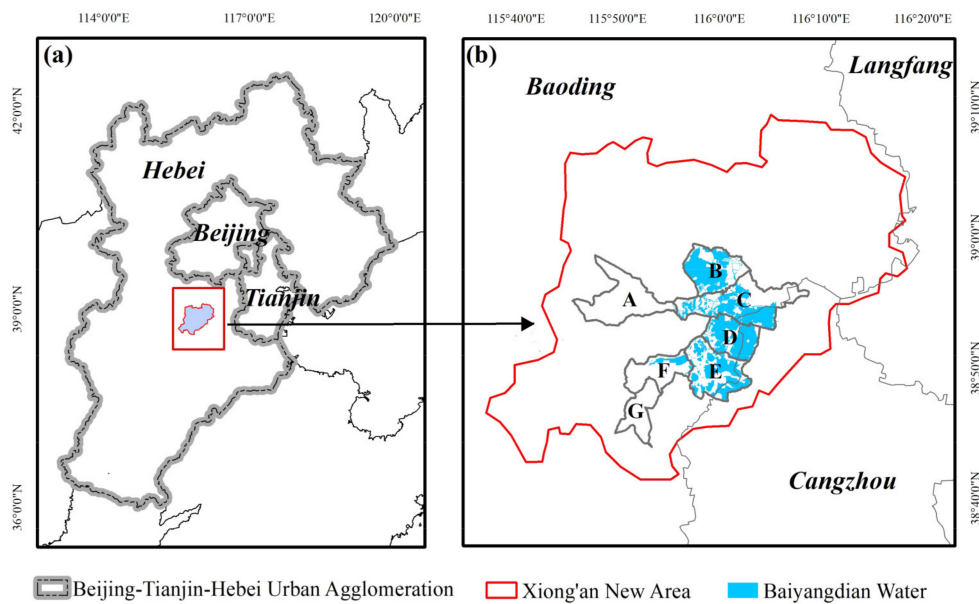


Figure 1. Location and distribution map of the study area. (a) The location of the Xiong’an New Area in the Beijing–Tianjin–Hebei Urban Agglomeration, China. (b) The location of Baiyangdian in Xiong’an New Area. A, B, C, D, E, F, and G are the seven main subregions of Baiyangdian Lake. The blue region is the surface water derived from the land cover dataset.

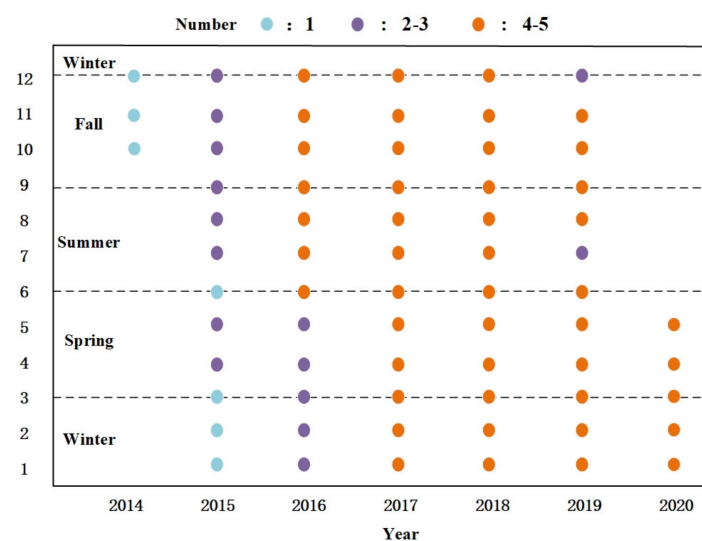


Figure 2. Temporal distribution of Sentinel-1 images from 24 October, 2014 to 28 May, 2020 used in this study. In terms of the number of images covering the study area, the blue dots represent only one image in the month, the purple dots represent 2–3 images, and the orange dots represent 4 to 5 images.

2.3. Methodology

2.3.1. Technical Framework

The data processing in this paper was divided into three steps, namely, image preprocessing, water extraction and accuracy verification, and analysis of temporal and spatial changes in Baiyangdian water. Based on the GEE platform, image preprocessing and water extraction were performed, and the rest of the work was completed in the local platform software (Figure 3). Specifically, the methods used were as follows: (1) perform image preprocessing such as band selection, noise filtering, and image masking for GRD images of multi-time sequence Sentinel-1; (2) extract Baiyangdian Lake’s surface water body by the automatic threshold method based on the OTSU method according to the grey value of different images; (3) perform a comparative analysis with the existing Landsat-SMDPSO water dataset of Baiyangdian Lake based on optical remote sensing data in the same historical period, using visual interpretation to verify the accuracy of the water body extraction results for many years, and summarizing the changes of water body thresholds in different seasons; and (4) perform an analysis of the spatiotemporal dynamics of water body results, specifically including analyses of different years, different seasons, and different regions.

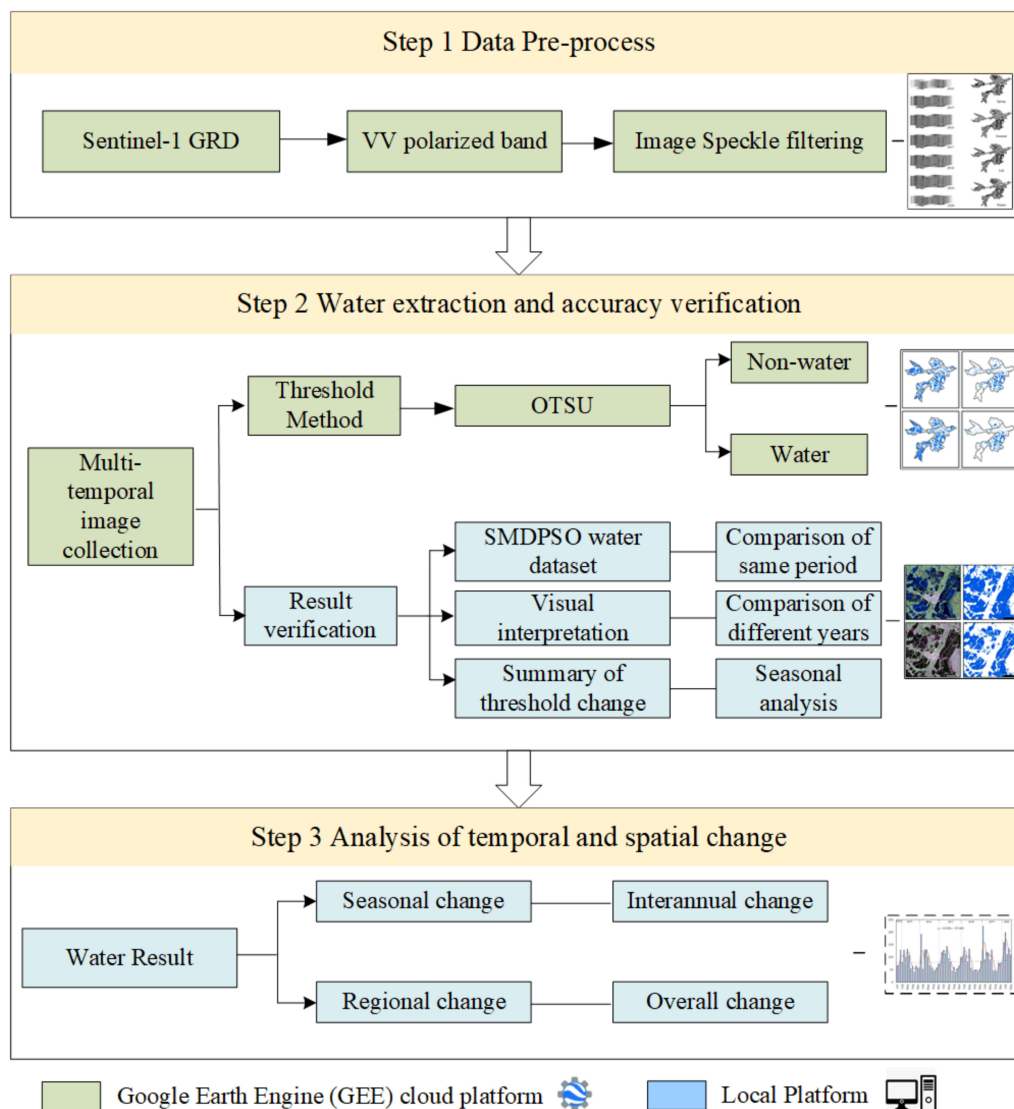


Figure 3. The technical framework diagram of this study.

2.3.2. Image Segmentation Method

The OTSU algorithm has been widely proven in the application of Sentinel-1 data. Because of its maturity and superiority compared with other algorithms, this paper uses the OTSU algorithm to extract water bodies [23–25]. The OTSU image segmentation method is used to automatically binarize the image based on clustering. OTSU assumes that the image can be segmented into two types of pixels, foreground and background, so it is necessary to calculate the best threshold that can separate the two types of pixels. Calculating the optimal threshold that can separate the two types of pixels and make the intraclass variance of the two types of pixels, the smallest and the largest between-class variance is required. The OTSU method proved that the results of minimizing the intraclass variance and maximizing the interclass variance are the same [26]. Therefore, only the maximum between-class variance is required. The equations are as follows:

$$\text{image} = \begin{cases} C_1, \text{ foreground} \\ C_2, \text{ background} \end{cases} \quad (1)$$

$$P_1M_1 + P_2M_2 = M, \quad (2)$$

$$P_1 + P_2 = 1, \quad (3)$$

where C_1 and C_2 are the two categories of the foreground and background of the hypothetical image segmentation, respectively. Then, P_1 and P_2 are the probabilities that the pixel is divided into C_1 and C_2 , M_1 and M_2 are the respective greyscale averages of the two types of pixels, and M is the image global mean value. Combined with the concept of variance between classes, the above equations can be simplified as follows:

$$\sigma(T)^2 = P_1P_2(M_1 - M_2)^2, \quad (4)$$

where T is the segmentation threshold of the foreground and background of the image, and $\sigma(T)^2$ is the between-class variance between the target and the background. Therefore, by traversing each grey level, the optimal grey value that can maximize the between-class variance $\sigma(T)^2$ is – the threshold T .

In Baiyangdian Lake, the surface backscatter coefficient histogram of the Sentinel-1 data has a bimodal structure in which the water body is specular reflection; its value is lower than that of land, and there is a clear distinction between land and water. The backscatter coefficient frequency distribution of the SAR images exhibits obvious “peak and valley” characteristics. When the value of a pixel is less than the selected optimal threshold, it can be determined that the pixel is water; otherwise, it is not water. Figure 4 shows the schematic diagram of the grey value histogram of the SAR image in the four seasons of spring, summer, fall, and winter, $T_1/T_2/T_3/T_4$, which are the optimum thresholds for the four seasons.

The equation expression is as follows:

$$\text{Class} = \begin{cases} \text{Water}, T_{dB} \leq T \\ \text{No Water}, T_{dB} > T \end{cases} \quad (5)$$

where Class is the feature category, T_{dB} is the backscattering coefficient value of the image, and T is the optimal threshold calculated by OTSU.

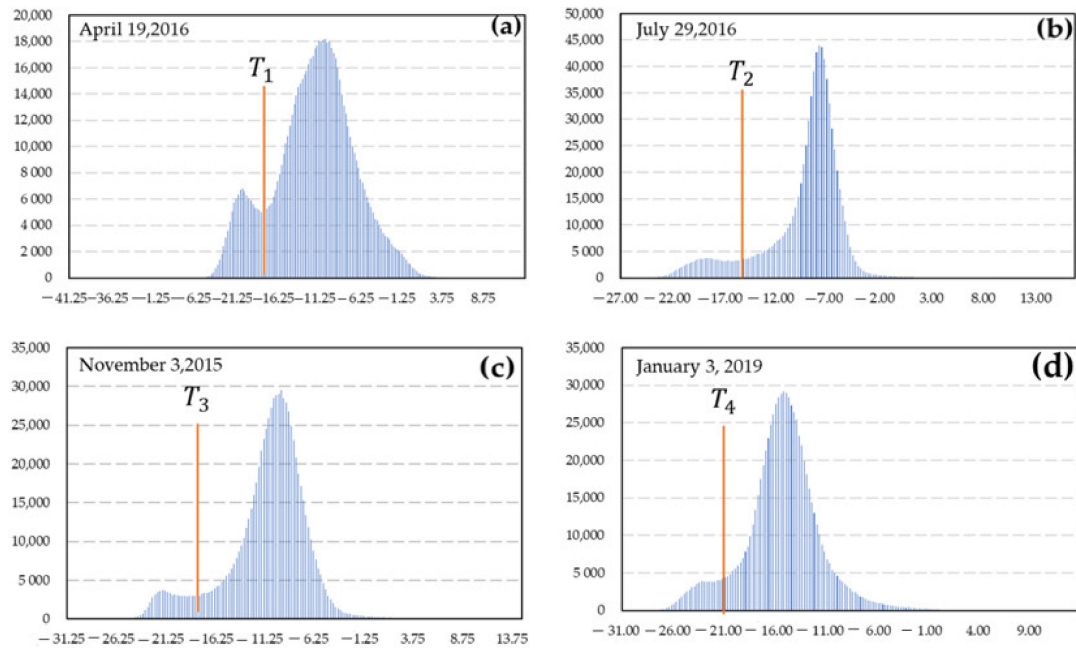


Figure 4. Schematic diagram of surface water threshold extraction from the Sentinel-1 image. Examples of the histogram of VV band in dB value. The four subpictures (a–d) are typical for the four seasons of spring, summer, fall, and winter. In each subpicture, the x-axis represents that the backscatter coefficient is calculated on the dB scale, the y-axis represents how many pixels have the same dB value in a bin, and the interval of bins is 0.25. $T_1/T_2/T_3/T_4$ are the best thresholds for the four images.

2.3.3. Water Inundation Frequency

Water inundation frequency (WIF) can reflect the spatial characteristics of Baiyangdian Lake. In this study, the WIF calculation method divides the number of times a pixel is marked as a water body by all the observations of each pixel. In this study, a total of 68 scenes of surface water extraction result images after monthly synthesis were used, so the number of observations per pixel was 68. The specific calculation equation is as follows:

$$WIF = \frac{\sum P_{i,j}}{N} \times 100\%, \quad (6)$$

where $P_{i,j}$ represents the pixels where the surface water appears at position (i, j) , $\sum P_{i,j}$ is the total number of times the water pixel appears at position (i, j) , and N is the total number of times the water pixel appears at that position.

2.3.4. Verification

To explore whether the water body extraction results were accurate, two methods were used for verification: (1) comparison and analysis of the extraction results with the existing Baiyangdian Lake water dataset, and (2) visual interpretation for verifying the accuracy of the extraction results by region. The water area of the entire study area and each subregion area were calculated separately, and the calculation equation is as follows:

$$A_i = N_i \times \text{Size}, \quad (7)$$

where A_i represents the area of water in a certain area, i refers to the different regions, N_i is the number of pixels in the area, and Size is the actual area corresponding to a pixel.

We used the relative error to calculate the error between the extracted water area and the actual water area.

$$R = (|A_e - A_a|/A_a) \times 100\%, \quad (8)$$

where R is the relative error between the extracted water area and the actual water area, A_e is the extracted water area, and A_a is the actual water area.

3. Results

3.1. Verification of Water Extraction Results in Baiyangdian Lake

To explore the accuracy of the surface water extraction results based on the Sentinel-1 and OTSU automatic threshold algorithm, the water body extraction results in this study were compared with an existing Landsat-SMDPSO water dataset for Baiyangdian Lake. The contrast images were imaged at the same historical time on 28 September, 2017. In Figure 5, A1 and A2 are Landsat-7 false-color composite images and Sentinel-1 false-color composite images, respectively. The darker color in the image represents the water body, and the reddish color is the impervious surface shown in image A2. B1 is the existing Landsat water body dataset based on the SMDPSO algorithm. B2 shows the water body extraction results of Sentinel-1 based on the OTSU algorithm. By comparison, the results of the two water bodies have a higher consistency in the overall distribution of Baiyangdian Lake; C1 and C2 are a partial enlargement of the original image, and the location is near the junction of subregions D and E, including towns, roads, ponds, and farmland. D1 and D2 are the water body extraction results corresponding to C1 and C2. Through comparison, it is found that the water body dataset based on Sentinel-1 can extract image detail information more finely, such as the pond ridges and field ridges beside the farmland, as well as some finely broken ponds and narrow river channels. It effectively divides the boundary between the construction land and the water body and effectively removes the misclassified and omitted results caused by the coarse resolution.

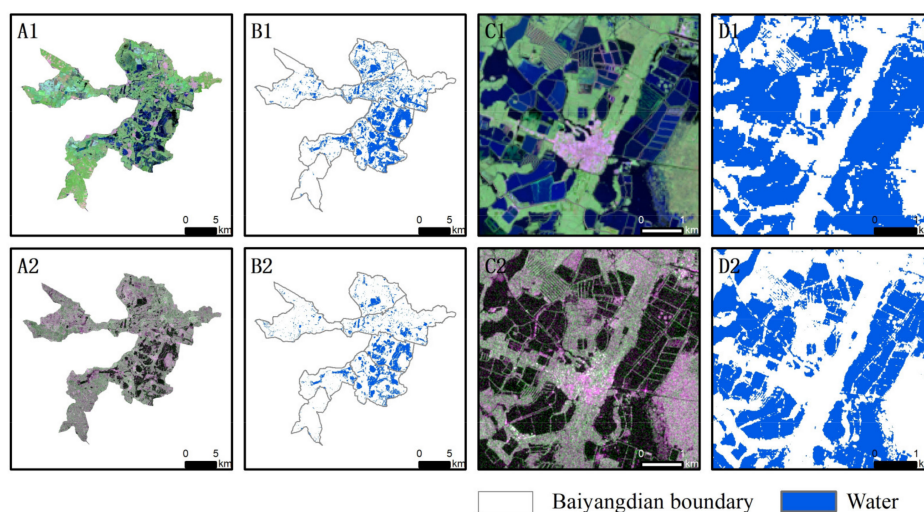


Figure 5. Comparison of Sentinel-1 surface water extraction and Landsat-SMDPSO datasets. (A1,A2) are the original images; (B1,B2) are the water extraction result; (C1,C2) are original images which are partially enlarged; (D1,D2) are the water extraction result corresponding to (C1,C2). (A1,A2,C1,C2) images were displaced by false-color (R, band 7; G, band 5; B, band 3 for Landsat-7, and R, VV; G, VH; B, VV for Sentinel-1).

To further test the accuracy of the extraction results of the seasonal water bodies, three areas in western, southern, and eastern portions of Baiyangdian Lake are selected as the study areas (Figure 6). On the left, the red, yellow, and blue polygonal areas are the selected sample areas. The same color corresponds to the same position and the corresponding year in the picture on the right. The red, yellow, and blue polygons are the boundaries of the water body extraction results in 2015/2017/2019, respectively. The water body extraction results in different years and different seasons are highly consistent with the original image, but the results extracted in winter are slightly different from the original area. It can be further found that the extraction results sufficiently to eliminate the influence of lotus and

reed covering the surface of the water body in the spring, summer, and fall. The boundary information is extracted accurately, and the land and water bodies are accurately divided. The winter extraction is somewhat different, such as the winter of 2017, which is affected by ice and snow, which may make the extracted water body larger than the real water body.

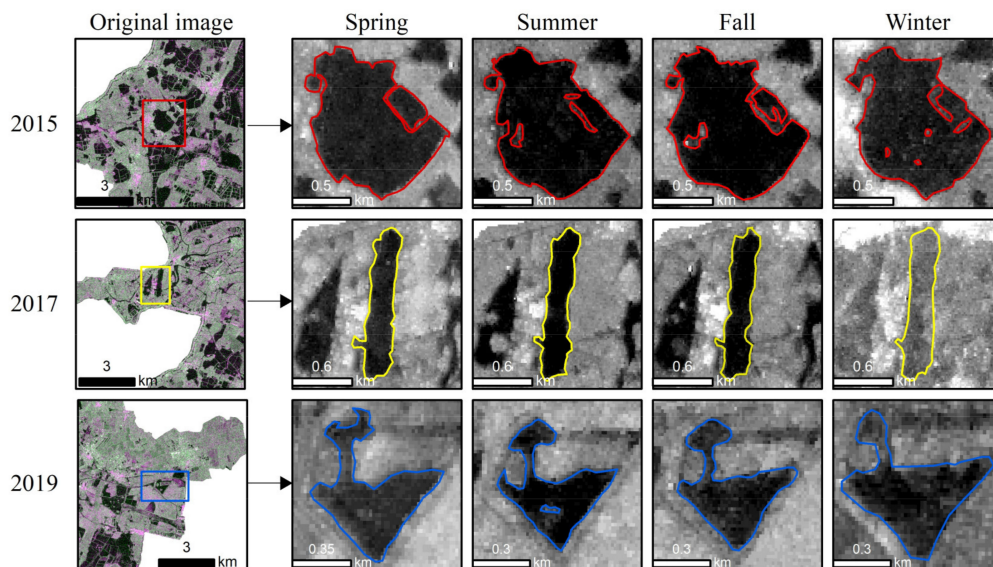


Figure 6. Seasonal validation of surface water extraction results with selected data and sample areas. The left side of the picture was displaced by false color images (R, VV; G, VH; B, VV). The red, yellow, and blue polygons are the sample areas selected in 2015, 2017, and 2019, respectively.

We use the relative error to characterize the difference between the extraction and visual interpretation results (Figure 7). In the spring, summer, and fall of 2015/2017/2019, the relative error of water extraction is small, most of which are less than 5%; the relative errors in the spring are 3.2%, 2.9%, and 1.7%, the relative errors in the summer are 4.6%, 4.1%, and 4.7%, and the relative errors in the fall are 4.3%, 2.5%, and 3.7%, respectively. However, in winter, the relative errors are large, 9.7%, 12.3%, and 13.2%, respectively. Vegetation growing on the water surface in summer and fall may have slightly affected the area of the extracted water body (red, yellow and blue polygons). Therefore, when using Sentinel-1 images to extract surface water bodies, spring is the best selection, summer and fall are the next best choice, and winter is the most challenging.

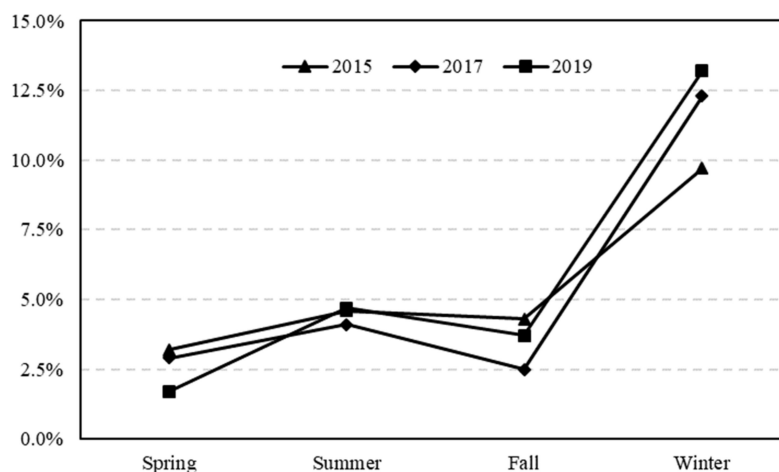


Figure 7. The relative error between the extracted water area and the actual water area.

To explore the changes in the surface water body thresholds in different seasons, the optimal water extraction thresholds were obtained from Sentinel-1 images in different seasons. This paper is based on 251 images and counts the thresholds of different seasons from 2014 to 2020. The threshold in summer is the largest (Figure 8). The second-largest occurs in the spring and fall. The winter threshold is the smallest and clearly differs from the first three. The average water threshold is -13.97 dB in summer, -14.45 dB in spring, -14.78 dB in fall, and -16.32 dB in winter. The water body in winter differs the most. Possibly due to the influence of ice, snow, and moist soil, the water threshold in winter is much smaller at approximately -1.5 dB than the water threshold in other seasons.

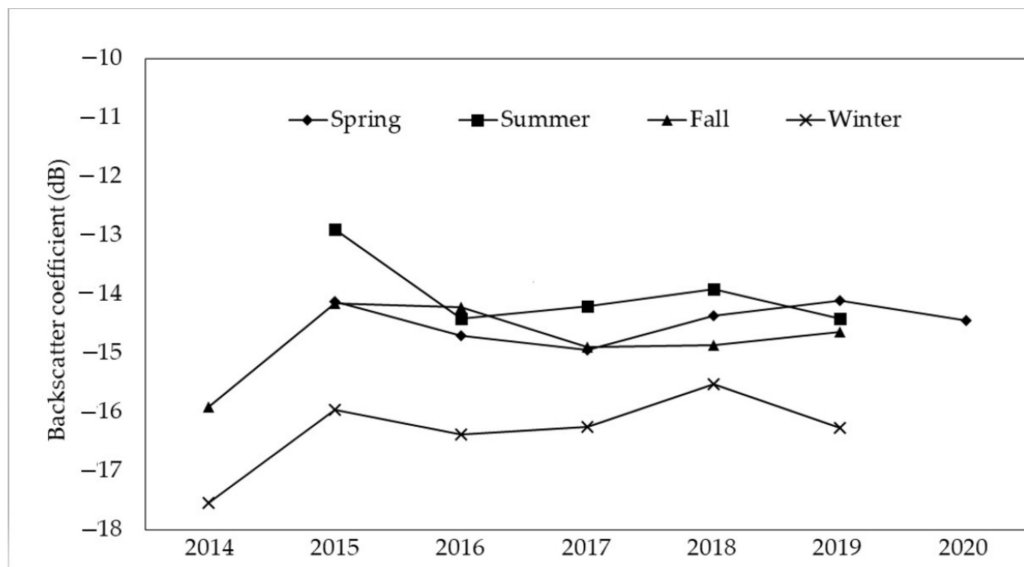


Figure 8. Seasonal law of water extraction threshold.

3.2. Analysis of Temporal Dynamic Change in Baiyangdian Lake

The purpose of establishing the SDG 6.6.1 indicators is to promote the protection and governance of the water environment through long-term monitoring of water-related ecosystems. For this goal, we processed Sentinel-1 data in multiyear and four-season water body images. In Figure 9, the vertical direction shows spring, summer, fall, and winter, and the horizontal change is seven years from 2014 to 2020. Generally, the water area in spring and winter is larger, and the water area in summer and fall is smaller. The winter of 2018 had the highest number of surface water bodies. Regardless of spring, summer, fall, or winter, water bodies are mainly distributed in the central region of Baiyangdian Lake, while those in the south and west are smaller.

As shown in Figure 10a, from the perspective of the same season across different years, there are more water bodies in spring and winter (December–May of the following year), and the total area is larger than that in summer and fall (June–November). The average water area in spring is 116 km^2 from 2015 to 2020, the average water area in summer is 64 km^2 from 2015 to 2019, the average water area in fall 2014–2019 is 58 km^2 , and the water area in winter is 118 km^2 from 2014 to 2019. The water area is relatively stable and shows little volatility in spring. The water area fluctuates in summer and fall. This may be affected by the growth of vegetation or the presence of moist soil, which may cause the extraction of water bodies to be affected by non-aqueous factors. The surface water of Baiyangdian Lake is at its most abundant in winter. Over the past six years, from 2014 to 2019, the area of water bodies has continued to grow, which may be due to the positive impact of the winter water replenishment from the “Yellow River to Baiyangdian Project”.

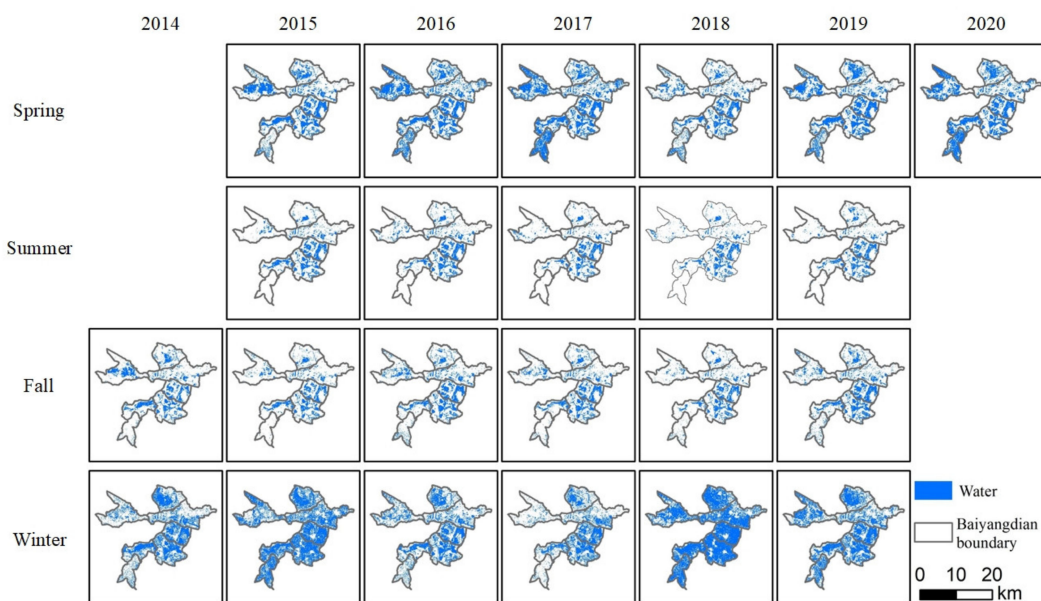


Figure 9. The seasonal surface water body distribution of Baiyangdian Lake from 2014 to 2020.

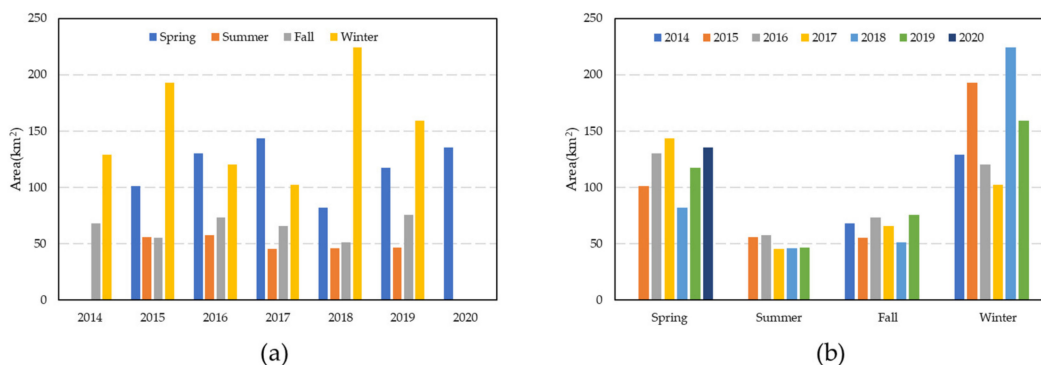


Figure 10. Seasonal changes in the water area of Baiyangdian Lake from 2014 to 2020. (a) The change in the water area in the same season in different years. (b) The change in water area in different seasons in the same year.

As shown in Figure 10b, from the perspective of different seasons in the same year, spring and winter water bodies have an absolute advantage in terms of area. The fall of 2018 had the smallest water body area of 47.52 km², and winter 2019 had the largest water body area of 146.18 km². The average water area is 88.10 km² in 2015, 86.22 km² in 2016, 87.30 km² in 2017, 84.72 km² in 2018, and 99.03 km² in 2019. Due to an insufficient number of samples in 2014 and 2020, they are not included in the statistical scope.

The SDG 6.6.1 regulations focus on the changing extent of water-related ecosystems over time. Therefore, we analyzed the change in the maximum and minimum extents of the water body of Baiyangdian Lake in each natural year from 2014 to 2020 (Figure 11). Through analysis, it was found that the largest water body in each natural year appeared on 31 December, 2014 (winter), 24 May, 2015 (spring), 14 January, 2016 (winter), 25 April, 2017 (spring), 19 February, 2018 (winter), 9 January, 2019 (winter), and 21 February, 2020 (winter); the smallest water bodies appeared on 18 October, 2014 (fall), 16 September, 2015 (fall), 15 September, 2016 (fall), 17 September, 2017 (fall), 17 October, 2018 (fall), 19 September, 2019 (fall), and 28 May, 2020 (spring). Data from October to December 2014 and January to June 2020 are available that do not cover the complete year, so using the data of these two years to analyze the time of the largest and smallest water bodies in each year may not be representative. Therefore, it can be concluded that the largest water body generally

appears in the winter period of the year, from December to February of the following year; the smallest water body appears in the fall of the year, from September to November.

To explore the overall variation in the water body area in Baiyangdian Lake from 2014 to 2020, as shown in Figure 12, the water body area was counted for 68 months. The water area of Baiyangdian Lake changes seasonally, with a small water area in the middle of the year and a large water area at the beginning and end of the year. Thanks to the regular replenishment mechanism of Baiyangdian Lake and the annual water replenishment volume exceeds 100 million m³, which makes up for the defect of large evapotranspiration. Therefore, the overall water body area has shown an upward trend, and the contribution of winter water replenishment has been particularly significant in recent years. The largest water body appears on 19 January, 2019, reaching 224.1 km², and the smallest water body appeared on 18 October, 2018, reaching 41.24 km².

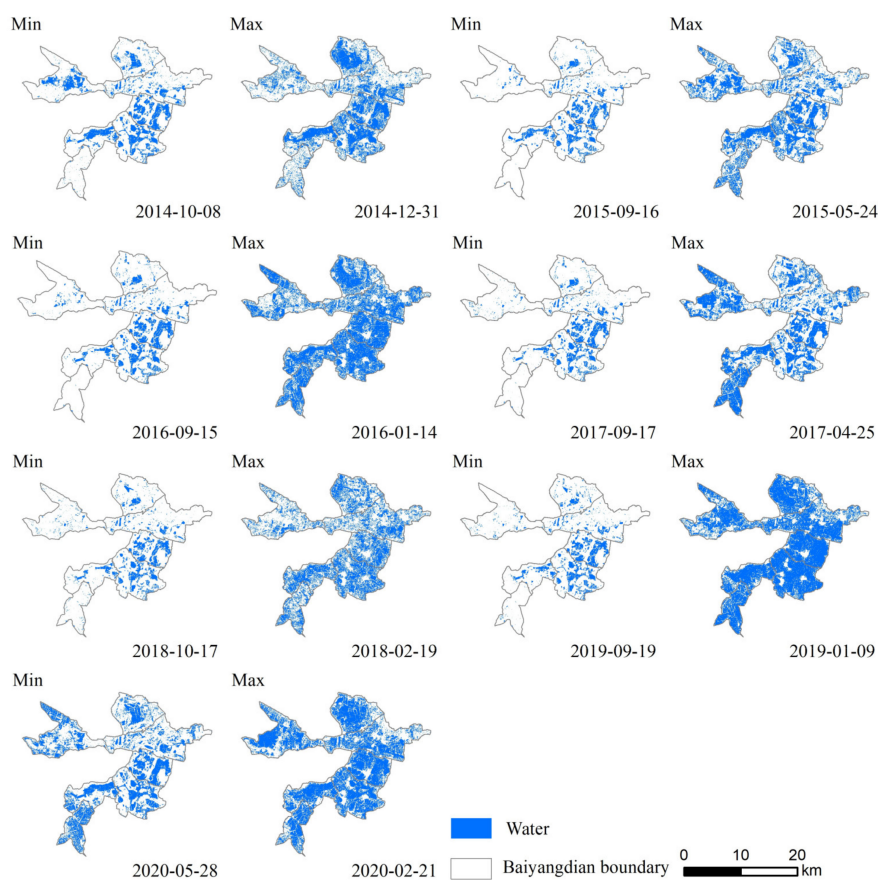


Figure 11. The maximum/minimum surface water area of Baiyangdian Lake among each year from 2014 to 2020.

3.3. Analysis of Spatial Dynamic Change in Baiyangdian Lake

In accordance with the SDG 6.6.1 guidelines, we explored the changes in the spatial distribution of the Baiyangdian Lake water body in the subregions, and the percentage of the water body area in the total water body area in each lake area was calculated. From Figure 13, it can be seen that over the past seven years, C, D, and E accounted for 57% of the total water area, and in summer, the water area of these three lakes accounted for more than 70% of the total water area, which is the main water storage area of Baiyangdian Lake. In summer, A and G account for less than 10% of the total water body. The average percentages of the total water area of each subregion lake are as follows: A 14.07%, B 11.76%, C 15.7%, D 20.17%, E 21.4%, F 11.24%, and G 5.67%.

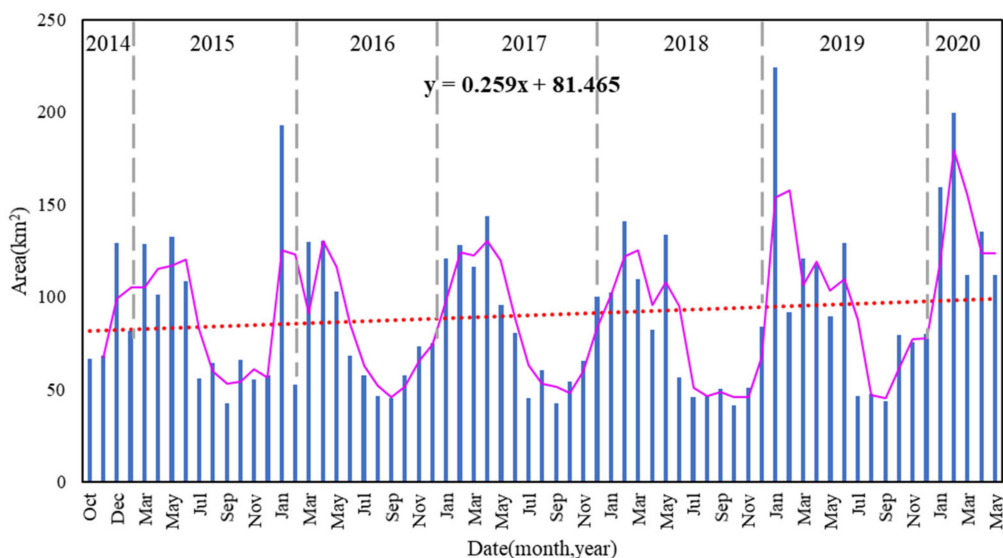


Figure 12. The overall change trend of surface water area in Baiyangdian Lake from 2014 to 2020. The red line is the linear trend of water body changes. The purple curve is the periodic law of water body area change.

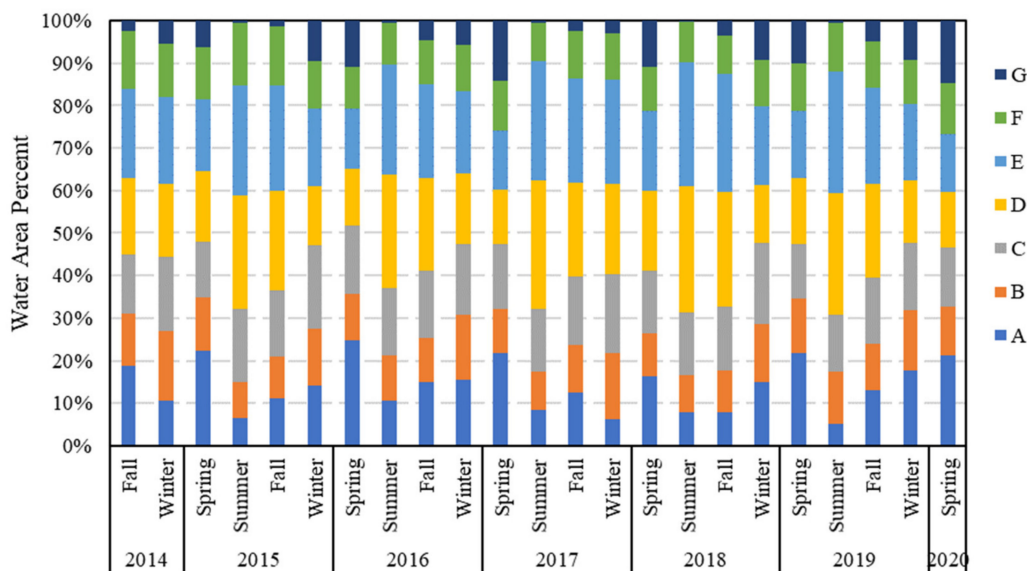


Figure 13. The percentage of each subregion(A–G) to the total water area. Different color patches represent different subregions. For reference, the percentage of D (yellow patches) refers to the water area of each season divided by the water area of the entire Baiyangdian Lake from 2014 to 2020.

Through calculations, trend graphs of the water area in the seven major subregions are produced. As shown in Figure 14, the seven subregions all show an upward trend. Among them, B, C, D, E, and F have a slower upward trend, while the water areas of A and G have a more obvious upward trend. In summer, the water areas of A and G are small, with an average value of less than 5 km². In winter, the water area is much greater than that in other seasons. The overall upward trend has elevated. The water areas of D and E show little change in all seasons.

The water area from largest to smallest by region is E, D, C, A, B, F, and G. The total area of the study area is 319.02 km², and the proportion of seasonal water area in the study area is in descending order winter, spring, fall, then summer. The total water area in winter accounts for the largest proportion, reaching 48.50%. The summer is the smallest, reaching only 15.73% (Table 1).

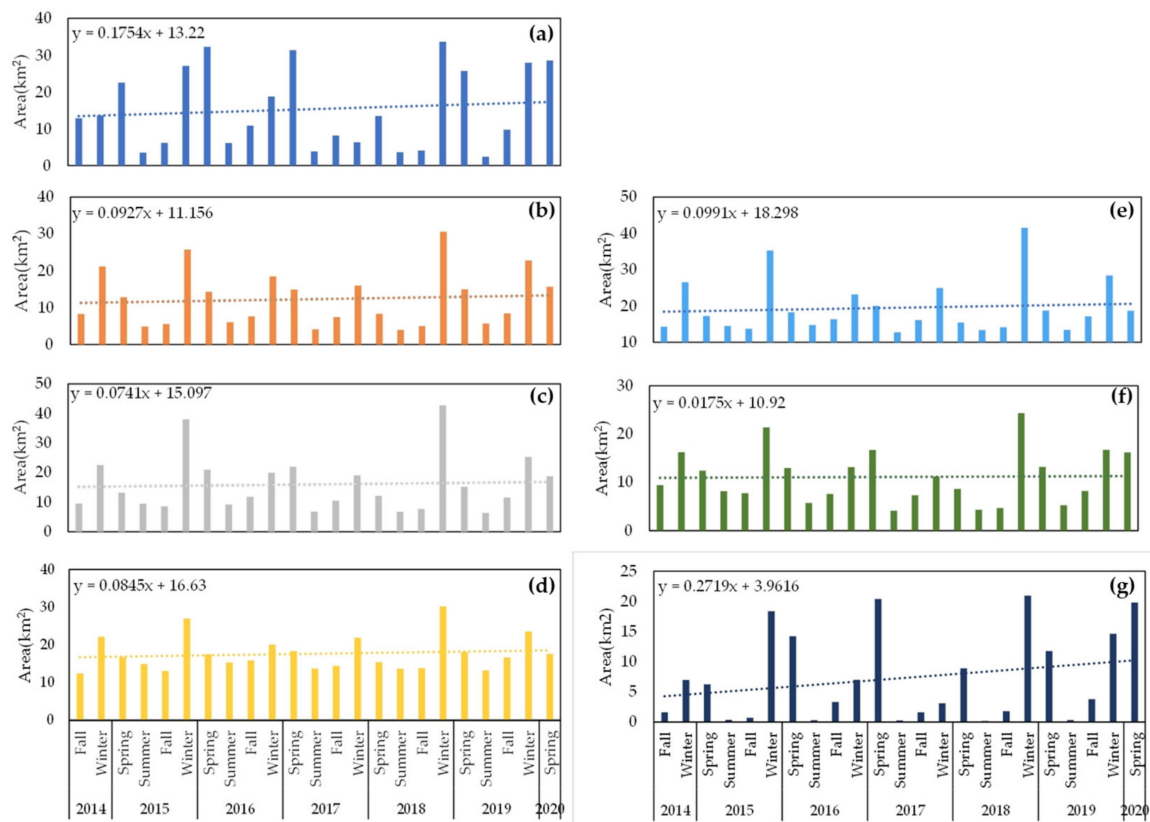


Figure 14. Dynamic trend of water area in the Baiyangdian Lake subregions. Pictures (a–g) represent subregion A to subregion G in sequence.

Table 1. The seasonal water area in Baiyangdian Lake subregions (km²).

	A	B	C	D	E	F	G	Total Area	Percent
Spring	25.63	13.47	17.02	17.29	18.03	13.37	13.54	118.35	37.10%
Summer	3.90	4.91	7.69	14.18	13.73	5.53	0.25	50.19	15.73%
Fall	8.64	7.03	9.93	14.38	15.27	7.50	2.12	64.86	20.33%
Winter	21.22	22.43	27.93	24.15	29.96	17.19	11.83	154.70	48.50%
Multi-year mean value	14.85	11.96	15.64	17.50	19.25	10.90	6.93	97.03	30.42%

In accordance with the requirements of the SDG 6.6.1 specifications, we used the water inundation frequency (WIF) to analyze the spatial extent of Baiyangdian Lake from 2014 to 2020. We divided the WIF into five levels: 0–20%, 20–40%, 40–60%, 60–80%, and 80–100%. The permanent water bodies (WIF > 60%) were mainly concentrated in subregions B, C, D, E, and F. There are many small lakes in this area, which have a total area of 49.69 km². Temporary water bodies (20% < WIF < 60%) are concentrated in the west of A, north of B, southeast of F, and east of G, with an area of 97.77 km²; WIF < 20% can be regarded as non-water because non-water is distributed in farmlands and villages with high consistency. These areas mainly appear in A, the northern portion of C, and most of G, with an area of 171.55 km² (Figure 15).

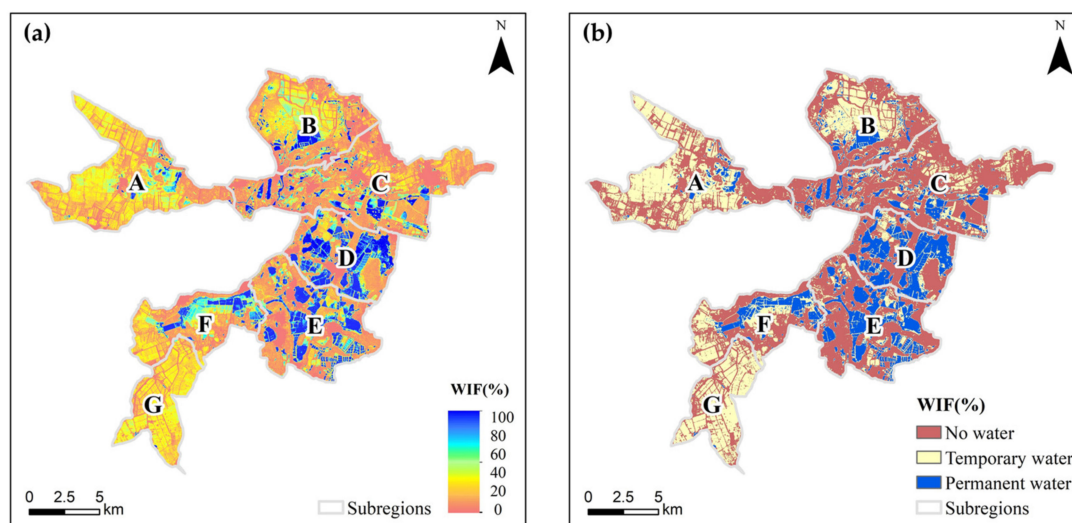


Figure 15. (a) Water inundation frequency (WIF) map of Baiyangdian Lake; (b) reclassified distribution map of different water body extents corresponding to picture (a).

4. Discussion

Comparing the trends of Baiyangdian Lake obtained in this paper with the results of other researchers, it is found that the changes have a high consistency pattern. In particular, Zhang et al. [37], Wang et al. [32], and Song et al. [38] have calculated the surface water area and the variation in the area of Baiyangdian Lake since 2008, which further verified the accuracy of the results from 2014 to 2020 in this study.

In addition, using the SDG 6.6.1 indicators and GEE platform for the rapid and accurate extraction of water, we analyzed different time scales (month and season), different water bodies (non-water, seasonal water, and permanent water), different water area ranges (maximum and minimum) and different regions. Compared with other studies, such as Shen et al. [36] and Yagmur et al. [37], this paper improves the spatiotemporal resolution of the Baiyangdian water map, increasing the spatial resolution to 10 m and the temporal resolution to monthly and seasonal time scales for estimating the SDG 6.6.1 indicators. Of great significance is that to better serve the SDG 6.6.1 indicator, we divided Baiyangdian Lake into seven main subregions and analyzed the water body area changes in each subregion and their different contributions to the whole Baiyangdian Lake.

Due to climate change and artificial water uses in recent years, the change in the Baiyangdian Lake water area has experienced four inflection periods in history. These periods include the dry period of 1984–1988, the declining period of 1989–2000, the steady period of 2000–2008, and the supplemental period that began in 2008 [32]. The slowly rising trend of the Baiyangdian Lake area from 2014 to 2020 obtained in this study conforms to this law. The possible reasons behind this are as follows: (1) in 2004, the Hebei Provincial Water Conservancy Bureau launched the “Yuecheng Reservoir to Baiyangdian Lake”, (2) in order to further alleviate the drying of the Baiyangdian Lake, since 2006, Baiyangdian has implemented several cross-basin “Diversion from the Yellow River to Baiyangdian Lake” water supplement measures, and (3) since the release of the “Baiyangdian Ecological Environment Management and Protection Plan (2018–2035)” in January 2019, ecological protection and water conservation areas have been established, and the “Diversion from the Yellow River to the Baiyangdian Lake” and the “Water Supply to the East of Baiyangdian Lake” projects have been established as a normal and stable water replenishment mechanism. The water supplement period of the Baiyangdian Lake is generally from November to February of the following year, which is why the water area is high in spring and winter in the results of this paper.

There are still some limitations to our study. The first limitation involves the extraction of seasonal water bodies. There are fewer water bodies extracted in summer and fall, which is not in line with the perception that the water surface area should increase as a result of rainfall occurring in summer and fall. This might be due to the growth of emergent plants and floating plants, meaning that the moist soil cover is blocked during remote sensing interpretation, and the extracted area of the water body will be smaller. The relative error is large because it is affected by ice and snow in winter. The second limitation lies in the lack of sufficient in-depth analysis of the causes of Baiyangdian water body changes. Baiyangdian Lake is located in the hinterland of the Xiong'an New Area, and its surrounding environment is complicated. It is greatly affected by climate change and human activities, making it very difficult to analyze the cause and effect of Baiyangdian water area changes. In addition to analyzing implemented policies combined with multiple water replenishment projects, other factors, such as rainfall and temperature, have not been considered.

In future research, we will first conduct a quantitative analysis of the influencing factors of the Baiyangdian water body, not only a qualitative analysis. It is also necessary to enhance multifactor analyses to better explore the factors influencing the Baiyangdian water body. Second, in terms of data sources, we will introduce multiple remote sensing data sources, such as Landsat-8, Sentinel-2, etc., to eliminate the factors influencing the Baiyangdian Lake vegetation and soil in summer and fall and ice and snow factors in winter. Therefore, we can analyze the Baiyangdian Lake water body changes more comprehensively to better address the SDG 6.6.1 indicators.

5. Conclusions

Using the GEE platform to address the SDGs, we developed an automatic water extraction framework using long-term Sentinel-1 images and the OTSU algorithm and analyzed water extent changes in Baiyangdian Lake from October 2014 to May 2020 in support of reporting SDG 6.6.1 indicators. Through visual interpretation and data comparison, the accuracy of the results was verified. We were able to quickly and accurately explore the spatiotemporal characteristics of Baiyangdian Lake and discuss the possible mechanisms driving these changes. In general, this study can draw the following conclusions:

- (1) The water area of Baiyangdian Lake showed a slow upward trend during the seven years from 2014 to 2020. Based on guidelines from SDG 6.6.1, the average water body area was 97.03 km². Among them, the water area of Baiyangdian Lake reached its peak due to the water supply to Baiyangdian Lake through the Yellow River diversion and upstream reservoirs at the end of 2018 and the beginning of 2019, and the largest water body appeared on 19 January 2019, reaching 224.1 km². In contrast, the smallest water body appeared on 18 October 2018, reaching 41.24 km².
- (2) In the three seasons of spring, summer and fall, due to the obvious difference in the backscattering coefficient values between different surface objects, the relative error of water extraction was small, at less than 5%, and the extraction effect in spring was the best. However, in winter, the mixture of ice, snow, and water made it more challenging to extract water, and the water extraction threshold was significantly smaller than approximately -1.5 dB in the other three seasons.
- (3) Based on the SDG 6.6.1 guidelines, the Baiyangdian Lake water body showed obvious seasonal characteristics. The water area in winter was the largest, with an average value of 154.70 km², while the water area was the smallest in summer, with an average value of 50.19 km². Subregions C, D, and E accounted for an average of 57% of the total water area. In summer, the water area of these three subregions accounted for over 70% of all water storage area and was the main water storage area of Baiyangdian Lake. Permanent water bodies are concentrated in subregions B, C, D, E, and F, with a total area of 49.69 km².

In short, based on the framework we developed in this study combined with the analysis of the characteristics of the temporal and spatial changes outlined in the SDG

policy, a solid foundation has been laid for further analysis of the extent and causes of changes in Baiyangdian Lake, as well as the promotion of water resource protection and regional management to achieve the SDG 6.6.1 indicators.

Author Contributions: Conceptualization, W.J.; methodology, Z.J. and X.W.; software, Z.J.; validation, W.J. and Z.L.; formal Analysis, Z.J.; investigation, Z.J. and C.W.; resources, Z.J.; data curation, Z.J.; writing-original draft preparation, Z.J.; writing-review and editing, W.J. and Z.L.; visualization, Z.J.; supervision, W.J. and K.P.; project administration, W.J.; funding acquisition, W.J. and Z.L. All authors have read and agreed to the published version of the manuscript.

Funding: This work was funded by the National Key Research and Development Program of China (2016YFC0503002), the National Natural Science Foundation of China (42071393), and Beijing Laboratory of Water Resources Security.

Informed Consent Statement: Informed consent was obtained from all subjects involved in the study.

Data Availability Statement: The data that support the findings of this study are available from the corresponding author upon reasonable request.

Acknowledgments: Appreciation goes to the editors and reviewers for their valuable comments that have helped to improve this paper.

Conflicts of Interest: The authors declare no conflict of interest.

References

- Gardner, R.C.; Finlayson, M. *Global Wetland Outlook: State of the World's Wetlands and Their Services to People 2018*; Secretariat of the Ramsar Convention: Gland, Switzerland, 2018.
- Pekel, J.-F.; Cottam, A.; Gorelick, N.; Belward, A.S. High-resolution mapping of global surface water and its long-term changes. *Nature* **2016**, *540*, 418–422. [[CrossRef](#)] [[PubMed](#)]
- Peng, K.; Jiang, W.; Deng, Y.; Liu, Y.; Wu, Z.; Chen, Z. Simulating wetland changes under different scenarios based on integrating the random forest and CLUE-S models: A case study of Wuhan Urban Agglomeration. *Ecol. Indic.* **2020**, *117*, 106671. [[CrossRef](#)]
- Fitoka, E.; Tompoulidou, M.; Hatziiordanou, L.; Apostolakis, A.; Höfer, R.; Weise, K.; Ververis, C. Water-related ecosystems' mapping and assessment based on remote sensing techniques and geospatial analysis: The SWOS national service case of the Greek Ramsar sites and their catchments. *Remote Sens. Environ.* **2020**, *245*, 111795. [[CrossRef](#)]
- Weise, K.; Höfer, R.; Franke, J.; Guelmami, A.; Simonson, W.; Muro, J.; O'Connor, B.; Strauch, A.; Flink, S.; Eberle, J.; et al. Wetland extent tools for SDG 6.6.1 reporting from the Satellite-based Wetland Observation Service (SWOS). *Remote Sens. Environ.* **2020**, *247*, 111892. [[CrossRef](#)]
- Mulligan, M.; van Soesbergen, A.; Hole, D.G.; Brooks, T.M.; Burke, S.; Hutton, J. Mapping nature's contribution to SDG 6 and implications for other SDGs at policy relevant scales. *Remote Sens. Environ.* **2020**, *239*, 111671. [[CrossRef](#)]
- Tulbure, M.G.; Broich, M.; Stehman, S.V.; Kommareddy, A. Surface water extent dynamics from three decades of seasonally continuous Landsat time series at subcontinental scale in a semi-arid region. *Remote Sens. Environ.* **2016**, *178*, 142–157. [[CrossRef](#)]
- Schaffer-Smith, D.; Swenson, J.J.; Barbaree, B.; Reiter, M.E. Three decades of Landsat-derived spring surface water dynamics in an agricultural wetland mosaic; Implications for migratory shorebirds. *Remote Sens. Environ.* **2017**, *193*, 180–192. [[CrossRef](#)]
- Donchyts, G.; Baart, F.; Winsemius, H.; Gorelick, N.; Kwadijk, J.; van de Giesen, N. Earth's surface water change over the past 30 years. *Nat. Clim. Chang.* **2016**, *6*, 810–813. [[CrossRef](#)]
- Sulla-Menashe, D.; Gray, J.M.; Abercrombie, S.P.; Friedl, M.A. Hierarchical mapping of annual global land cover 2001 to present: The MODIS Collection 6 Land Cover product. *Remote Sens. Environ.* **2019**, *222*, 183–194. [[CrossRef](#)]
- McFeeters, S.K. The use of the Normalized Difference Water Index (NDWI) in the delineation of open water features. *Int. J. Remote Sens.* **1996**, *17*, 1425–1432. [[CrossRef](#)]
- Xu, H. Modification of normalised difference water index (NDWI) to enhance open water features in remotely sensed imagery. *Int. J. Remote Sens.* **2006**, *27*, 3025–3033. [[CrossRef](#)]
- Feyisa, G.L.; Meilby, H.; Fensholt, R.; Proud, S.R. Automated Water Extraction Index: A new technique for surface water mapping using Landsat imagery. *Remote Sens. Environ.* **2014**, *140*, 23–35. [[CrossRef](#)]
- Fisher, A.; Flood, N.; Danaher, T. Comparing Landsat water index methods for automated water classification in eastern Australia. *Remote Sens. Environ.* **2016**, *175*, 167–182. [[CrossRef](#)]
- Deng, Y.; Jiang, W.; Tang, Z.; Li, J.; Lv, J.; Chen, Z.; Jia, K. Spatio-Temporal Change of Lake Water Extent in Wuhan Urban Agglomeration Based on Landsat Images from 1987 to 2015. *Remote Sens.* **2017**, *9*, 270. [[CrossRef](#)]
- Zhang, L.; Weng, Q. Annual dynamics of impervious surface in the Pearl River Delta, China, from 1988 to 2013, using time series Landsat imagery. *ISPRS J. Photogramm. Remote Sens.* **2016**, *113*, 86–96. [[CrossRef](#)]
- Verpoorter, C.; Kutser, T.; Tranvik, L. Automated mapping of water bodies using Landsat multispectral data. *Limnol. Oceanogr. Methods* **2012**, *10*, 1037–1050. [[CrossRef](#)]

18. Du, Y.; Zhang, Y.; Ling, F.; Wang, Q.; Li, W.; Li, X. Water Bodies' Mapping from Sentinel-2 Imagery with Modified Normalized Difference Water Index at 10-m Spatial Resolution Produced by Sharpening the SWIR Band. *Remote Sens.* **2016**, *8*, 354. [[CrossRef](#)]
19. Tiner, R.W.; Lang, M.W.; Klemas, V.V. *Remote Sensing of Wetlands: Applications and Advances*; CRC Press: Boca Raton, FL, USA, 2015.
20. Aires, F.; Prigent, C.; Fluet-Chouinard, E.; Yamazaki, D.; Papa, F.; Lehner, B. Comparison of visible and multi-satellite global inundation datasets at high-spatial resolution. *Remote Sens. Environ.* **2018**, *216*, 427–441. [[CrossRef](#)]
21. Bioresita, F.; Puissant, A.; Stumpf, A.; Malet, J.-P. Fusion of Sentinel-1 and Sentinel-2 image time series for permanent and temporary surface water mapping. *Int. J. Remote Sens.* **2019**, *40*, 1–24. [[CrossRef](#)]
22. Navarro, J.C.V.; Salazar-Garibay, A.; Téllez-Quiñones, A.; Orozco-Del-Castillo, M.; López-Caloca, A.A. Inland water body extraction in complex reliefs from Sentinel-1 satellite data. *J. Appl. Remote Sens.* **2019**, *13*, 016524. [[CrossRef](#)]
23. Zeng, L.; Schmitt, M.; Li, L.; Zhu, X.X. Analysing changes of the Poyang Lake water area using Sentinel-1 synthetic aperture radar imagery. *Int. J. Remote Sens.* **2017**, *38*, 7041–7069. [[CrossRef](#)]
24. Markert, K.N.; Markert, A.M.; Mayer, T.; Nauman, C.; Haag, A.; Poortinga, A.; Bhandari, B.; Thwal, N.S.; Kunlaimai, T.; Chishtie, F.; et al. Comparing Sentinel-1 Surface Water Mapping Algorithms and Radiometric Terrain Correction Processing in Southeast Asia Utilizing Google Earth Engine. *Remote Sens.* **2020**, *12*, 2469. [[CrossRef](#)]
25. Zhou, S.; Kan, P.; Silbernagel, J.; Jin, J. Application of Image Segmentation in Surface Water Extraction of Freshwater Lakes using Radar Data. *ISPRS Int. J. Geo Inf.* **2020**, *9*, 424. [[CrossRef](#)]
26. Otsu, N. A threshold selection method from gray-level histograms. *IEEE Trans. Syst. Man Cybern.* **1979**, *9*, 62–66. [[CrossRef](#)]
27. Gorelick, N.; Hancher, M.; Dixon, M.; Ilyushchenko, S.; Thau, D.; Moore, R. Google Earth Engine: Planetary-scale geospatial analysis for everyone. *Remote Sens. Environ.* **2017**, *202*, 18–27. [[CrossRef](#)]
28. Deng, Y.; Jiang, W.; Tang, Z.; Ling, Z.; Wu, Z. Long-Term Changes of Open-Surface Water Bodies in the Yangtze River Basin Based on the Google Earth Engine Cloud Platform. *Remote Sens.* **2019**, *11*, 2213. [[CrossRef](#)]
29. Peng, K.; Jiang, W.; Deng, Y. Identification of wetland damage degree and analysis of its driving forces in Wuhan Urban Agglomeration. *J. Natl. Resour.* **2019**, *34*, 1694–1707.
30. Lv, J.; Jiang, W.; Wang, W.; Wu, Z.; Liu, Y.; Wang, X.; Li, Z. Wetland Loss Identification and Evaluation Based on Landscape and Remote Sensing Indices in Xiong'an New Area. *Remote Sens.* **2019**, *11*, 2834. [[CrossRef](#)]
31. Li, Z.; Jiang, W.; Wang, W.; Chen, Z.; Ling, Z.; Lv, J. Ecological risk assessment of the wetlands in Beijing-Tianjin-Hebei urban agglomeration. *Ecol. Indic.* **2020**, *117*, 106677. [[CrossRef](#)]
32. Wang, X.; Wang, W.; Jiang, W.; Jia, K.; Rao, P.; Lv, J. Analysis of the Dynamic Changes of the Baiyangdian Lake Surface Based on a Complex Water Extraction Method. *Water* **2018**, *10*, 1616. [[CrossRef](#)]
33. Jia, K.; Jiang, W.; Li, J.; Tang, Z. Spectral matching based on discrete particle swarm optimization: A new method for terrestrial water body extraction using multi-temporal Landsat 8 images. *Remote Sens. Environ.* **2018**, *209*, 1–18. [[CrossRef](#)]
34. Torres, R.; Snoeij, P.; Geudtner, D.; Bibby, D.; Davidson, M.; Attema, E.; Potin, P.; Rommen, B.; Floury, N.; Brown, M.; et al. GMES Sentinel-1 mission. *Remote Sens. Environ.* **2012**, *120*, 9–24. [[CrossRef](#)]
35. Lee, J.-S. Refined Filtering of Image Noise Using Local Statistics. *Refin. Filter. Image Noise Using Local Stat.* **1980**, *15*, 380–389. [[CrossRef](#)]
36. Yommy, A.S.; Liu, R.; Wu, S. SAR Image Despeckling Using Refined Lee Filter, Intelligent Human-Machine Systems and Cybernetics. In Proceedings of the 7th International Conference on Intelligent Human-Machine Systems and Cybernetics, Hangzhou, China, 26–27 August 2015; pp. 260–265.
37. Zhang, M.; Gong, Z.; Zhao, W. Analysis of driving forces of Baiyangdian wetland evolution during 1984–2013. *Chin. J. Ecol.* **2016**, *35*, 499–507.
38. Song, C.; Ke, L.; Pan, H.; Zhan, S.; Liu, K.; Ma, R. Long-term surface water changes and driving cause in Xiong'an, China: From dense Landsat time series images and synthetic analysis. *Sci. Bull.* **2018**, *63*, 708–716. [[CrossRef](#)]